ISSN: 2755-9351

Journal of Alzheimer's Disease & Reports

SCIENTIFIC Research and Community

Research Article

Open Access

Plant Polyprenols Disrupt the IP3R-GRP75-VDAC-MCU Axis to Restore Mitochondrial Motility Defects Associated with Alzheimer's Disease

Giorgio Dell'Acqua[1,2], Tony McFadden[1*], Beatrice Blanc[3,5], Romain MJ Lasseur[3,6], Nicolas Brouilly[4] and Nathalie A Compagnone[3,7*]

[1]Juvesen Pty Ltd, 60 Ludbrook Ave Caulfield South VIC 3162, Australia

[2]Present Address: Dellacqua Consulting LLC, 47 Mercer Street, Jersey City, NJ 07302, USA

[3]Translational Medicine Department, ICDD, 800 ave du chateau de Jouques, 13420 Gemenos, France

[4]Aix Marseille Univ, CNRS, IBDM, 13009, Marseille, France

[5]Present address: Beckman Coulter Immunotech, 130 Av de Lattre de Tassigny, 13009 Marseille

[6]Present Address: Department of Biochemistry and Molecular Biology, BioMedical Center, Faculty of Medicine, University of Iceland, Reykjavik, Iceland

[7]Present Address: mtBiolabs, Mitochondrial Cell Biology, 185 chemin des France, 13390 Auriol France

ABSTRACT

Standardized Plant Polyprenols (SPP) were shown to ameliorate cognitive function in a rat model of Alzheimer's Disease (AD) but we lack understanding of its mechanism of action. The increasing prevalence of AD with age makes it a major health burden in economically developed countries. Mitochondria dysfunctions are highly associated with the pathophysiology of AD. We aimed at better understanding the biological processes by which SPP target mitochondrial behavior and function to improve AD-associated phenotype in a patient-derived cell model. We found that SPP dose-dependently rescued AD-associated defects in mitochondrial motility, restoring docking capabilities in the "sentry" mitochondrial sub-population. SPP also restored mitochondrial bioenergetics, particularly increasing ATP production from the mitochondrial electron transfer chain. Rescue of the mitochondrial motility phenotype was independent from the SPP-mediated increase in de novo protein synthesis and reduced EIF2α activation. Instead we found that SPP modulated MAMs occurrence & signaling, engaged in the control of mitochondrial motility by modulating Ca^{2+} flux and ER-stress, both processes being impaired in AD. SPP limited the interactions between SERCA1 and the IP3R-GRP75-VDAC-MCU axis, which controlled mitochondrial Ca^{2+} flux. Disruption of the IP3R-GRP75-VDAC-MCU axis at MAMs by SPP provided a rationale for the control of mitochondrial movements and suggested a mechanism by which SPP increased bioenergetics efficiency and restored ATP production in AD-cells. Other biological processes that may explain SPP activity were discussed including the possibility that the TRACK-Miro interaction may be involved. Our data support clinical testing of SPP as a food supplement to sustain cognitive function in the elderly.

***Corresponding author's:**

Tony McFadden, Juvesen Pty Ltd, 60 Ludbrook Ave Caulfield South VIC 3162, Australia.

Nathalie A Compagnone, Translational Medicine Department, ICDD, 800 ave du chateau de Jouques, 13420 Gemenos, Present Address: mtBiolabs, Mitochondrial Cell Biology, 185 chemin des France, 13390 Auriol France.

Received: September 16, 2025; **Accepted:** September 20, 2025; **Published:** September 28, 2025

Keywords: Polyprenol, Alzheimer's Disease, Mitochondria, Mitochondria-ER Associated Membrane (MAM), Bioenergetics, Intracellular Calcium Flux

Introduction

For a long time, mitochondria have been reduced to their central bioenergetic role in eukaryotic cells, where they control the generation of Adenosine Triphosphate (ATP) from oxidation of nutrients. Yet, these organelles are highly dynamic. As such, they are motile and undergo fusion, fission and degradation processes in concert with the normal cell function. Because of their ability to affect local ATP and calcium concentrations, the sub-cellular distribution of mitochondria can also be extremely important. Studying mitochondrial behavior in health and disease thus carries important predictive value [1,2]. In recent years, this field has been extremely dynamic, resulting in a significant increase in our understanding of mitochondrial dynamics, biogenesis, transport and degradation [3-10]. It is now clear that structural and functional defects of the mitochondrial reticular network represent a hallmark of aging and are present in many human diseases, including Alzheimer's Diseases (AD) [11-13]. However, a careful morphofunctional classification of mitochondrial

dynamics is only partially eluded [14,15]. Further understanding of the complex association between mitochondrial function & behavior is needed. Here we report the use of mitochondrial behavior as a means to characterize the effect of a Standardized Plant Polyprenols Extract (SPP) in a fibroblasts model of AD. To provide functional associations with the observed phenotype we quantified cell bioenergetics, mtDNA content, *de novo* protein synthesis, ER-Stress markers and occurrence of contact points between ER and mitochondrial membranes at MAMs in healthy and in AD-cells, untreated and treated with 3 doses of SPP. We also measured amyloid fibrillation in the extracellular space and Tau-hyperphosphorylation, hallmark markers of the disease.

SPP, isolated from the green verdure of Picea Abies (L.) Karst, is a concentrate of pharmaceutical grade polyprenols (95% polyprenols or long chain isoprenoid alcohols) consisting of a series of homologues containing 8-20 isoprene units with the predominant isoprene units being from 13-18. SPP affect the isoprenoid pathway. It was previously described in Fedotova et al. It is a known antioxidant with anti-inflammatory, immunomodulatory and neuroprotectant properties similar to polyprenols extracted from Gingko Biloba [16]. It has been shown to ameliorate neurogenesis and oligodendrogenesis in a rat model of demyelination and cognitive functions in a rat model of AD, but its mechanism of action remains elusive [17,18]. Plant polyprenols, including SPP, are metabolized in vivo into dolichol. The phosphorylated from of dolichol (Dol-P), due to its hydrophobic properties, is the lipid carrier for glycosyl residues across membranes during glycosylation reactions and is embedded into the cytoplasmic surface of the ER membrane [19, 20]. Despite an increase in dolichol levels in the human brain up to age 70, these levels are reduced in brain regions affected by AD [21]. Dolichyl phosphate (Dol-P), an obligatory intermediate in the N-glycosylation process, is relatively unchanged during aging but has been shown to increase markedly in brains from patients with AD [21-23]. Recent glycomic analysis showed that the high level of (Hex)3(HexNAc)5(Fuc)1, an N-Glycan, was associated with protection of the brain of elderly subjects against β-amyloid deposition and Tau tangles, in a longitudinal study (The ROSEMAP study) [24]. N-linked glycans impact neuronal functions, including maintenance of resting membrane potential, axon firing and synaptic vesicle release. N-linked glycosylation is a central mediator of the Unfolded Protein Response (UPR), which determines neuronal cell fate [25]. More generally, N-linked protein glycosylation in the brain is metabolically channeled to glucosamine metabolism through glycogenolysis, suggesting a possible interaction with cell metabolism [26]. Moreover, altering O-Linked and N-acetylglucosamine cycling disrupts mitochondrial function and alters mitochondrial morphology [27,28]. In this paper we studied mitochondrial behavior and function to better understand biological processes affected by SPP-treatment in AD-cells.

Materials and Methods

Chemicals and antibodies resources used in this study are described in Table 1 (Supplementary information). Detailed methods can be found in the accompanying supplemental information.

Statistics

We analyzed the behavior of individual mitochondria in live cells. When characterizing the mitochondria motility, our study population was thus composed of individualized mitochondria (n). Other outcome measures were evaluated at the cell level. The number of cells analyzed and repeated platings were indicated in the figure legend for information. When considering continuous numeric variables, one-way ANOVAs were performed to compare the effect of treatment on the different outcome measures performed. ANOVAs were performed after a preliminary distribution analysis to assess normality of the data distribution. Normalization of the data was performed when necessary. To evaluate the differences between treatment groups, a Tukey's HSD Test for multiple comparisons was made. The effect of the treatment groups on non-continuous variables was analyzed with a X^2 test.

Results & Discussion

AD Reduces Docking Time in the "Sentry" Mitochondria Sub-Population and SPP-Treatment Rescues this Phenotype

Our study uses fibroblasts derived from human donors, a model that has been validated to recapitulate mitochondrial impairments found in the AD brain [12, 29–33]. We have found that sedentary mitochondria are overrepresented in fibroblasts obtained from AD patients consistent with reports from other groups [34-37]. Here, we focus on the docking process by which mitochondria stop in specific places to produce energy and control calcium homeostasis where needed. Mitochondria movements have been reported to be regulated by the ATP/ADT ratio, glucose gradients and by free cytosolic calcium concentrations [38-44]. However, the mechanisms that underpin mitochondria dynamism in link to their motility and function are yet to be fully understood.

As previously shown (submitted), in healthy cells, the mitochondrial motility behavior is heterogeneous. The mitochondrial motility behavior is defined by four different movement typologies:

- **Sedentary Workers** are mitochondria that constantly move for very short distances in Brownian movements, producing ATP at a specific site,
- **Traveling Workers** are mitochondria that adopt slow movements, occasionally docking where they produce ATP, moving at slightly higher speed when changing site but staying short distances from their original position.
- **Sentries** are mitochondria capable of traveling very long distances. They remain, however, a slow-moving population. They are characterized by spending time docked, in full arrest, when actively functionally engaged at specific sites (in this group, docking of the mitochondria occurs for at least 25–30% of the time during the recorded trajectory)
- **Explorers/Firefighters** are mitochondria that are characterized by frequent high-speed displacements. If mitochondria dock, they are in full arrest. We observed a 0.76-fold decrease in the arrest frequency in mitochondria in the AD-cells compared to mitochondria in healthy controls (p=0.0012, n=251). We found that the treatment group significantly modified the docking time in the mitochondrial population (p=0.0022, n=728) (Figure 1A).

Citation: Giorgio Dell'Acqua, Tony McFadden, Beatrice Blanc, Romain MJ Lasseur, Nicolas Brouilly, et al. (2025) Plant Polyprenols Disrupt the IP3R-GRP75-VDAC-MCU Axis to Restore Mitochondrial Motility Defects Associated with Alzheimer's Disease. Journal of Alzheimer's Disease & Reports. SRC/JADR-111.
DOI: doi.org/10.47363/JADR/2025(2)110

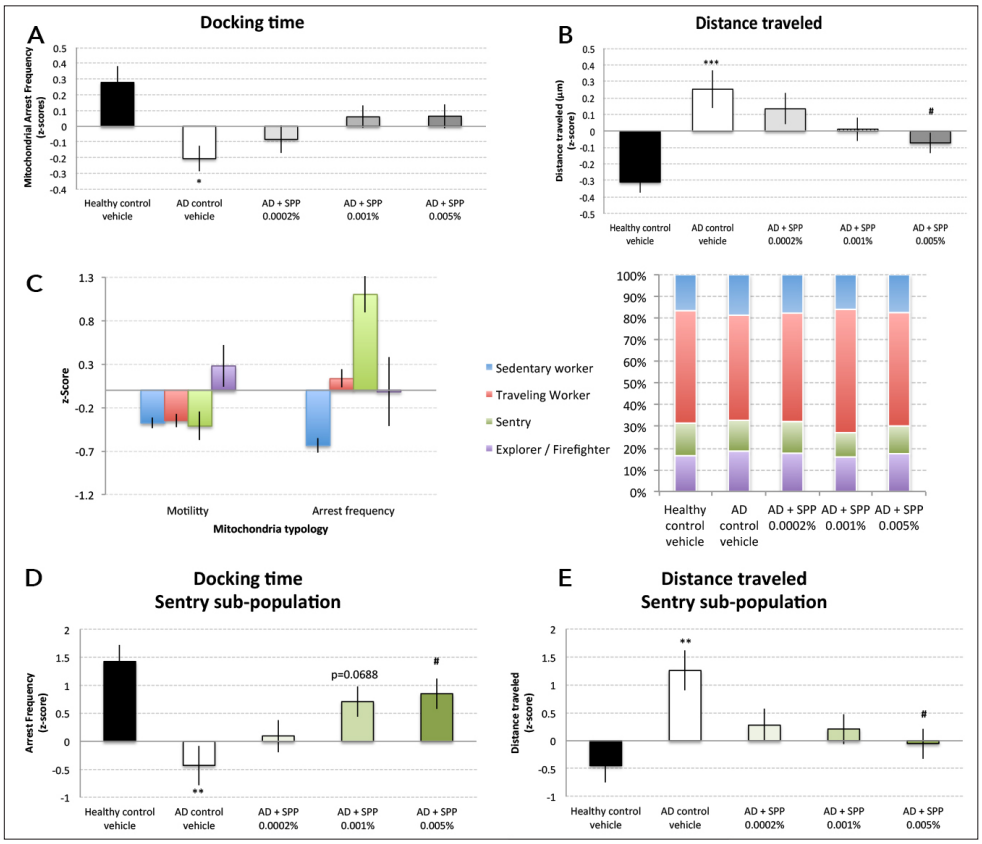

Figure 1: Analysis of the Motility Behavior of the Mitochondria in the Different Treatment Groups

A: Z-score for the docking time of individual mitochondria (whole population) – B: Z-score for the corresponding distance traveled (whole population) (n=728 individual mitochondria analyzed, cell number= 45, repeated platings=3); – C: (Left panel) profile for the different typology of movements observed. "Sedentary workers", "Travelling workers" and "Sentry" are mitochondria that have a motility below average, while "Explorer/Firefighters" have a motility higher than average. Arrest frequency discriminates the "Sentry" mitochondria from the rest of the population since they display the highest arrest frequency (a surrogate measure for docking time). Conversely, the lowest arrest frequency is seen in "Sedentary workers" that adopt Brownian movements. (Right panel) – Percent representativeness of the different sub-populations in the different experimental conditions. – D: Z-score for the docking time of individual mitochondria in the "Sentry" subpopulation – E: Z-score for the corresponding distance traveled in the "Sentry" subpopulation (n=194 individual mitochondria analyzed, cell number= 45, repeated platings=3).

To evaluate whether SPP extract modulated the mitochondrial phenotype associated with AD we treated AD-cells with 3 doses of SPP ranging from 0.0002% to 0.005% in DMSO. SPP was identified as partially reversing the mitochondrial phenotype associated with AD in a dose dependent manner (Figure 1). We measured the distance traveled during live cell imaging in the whole mitochondrial network (Figure 1B). When mitochondria dock, they do not travel. The distance traveled is thus inversely correlated to the docking time. We observed that the treatment group significantly impacted the distance traveled by mitochondria in the whole reticular network ($p \leq 0.0001$, n=728). AD significantly increased the distance traveled by individual mitochondria compared to that in healthy control cells by 1.42-fold ($p \leq 0.0001$, n=251), consistent with a reduced docking time. SPP-treatment dose-dependently reversed this effect, which reached significance when SPP was used at 0.005% (p=0.0365, n=306).

We observed no significant differences in the distribution of the mitochondrial sub-populations in response to the disease state (Figure 1C). Sentries represented 12–16% of the mitochondria in the different experimental groups (Figure 1C). However, this sub-population was particularly impacted by AD and responsive to the SPP-treatment. Changes in mitochondrial motility within the Sentry sub-population in AD-cells were mostly explained by the combination of a strong 0.42-fold reduction of the docking time (p=0.0004, n= 39) associated with a 2.17-fold increase in the distance traveled ($p \leq 0.0001$, n= 39) (Fig 1D, E). SPP, dose-dependently and significantly, yet only partially restored the normal phenotype. We observed a 1.96-fold increase (p=0.0053, n=39) in the docking time coupled to a 0.58-fold reduction in the distance traveled (p=0.0163, n=39) in this sub-population in response to 0.005% SPP (Figure 1 D,E).

This is the first evidence that using SPP to enhance dolichol precursors and impact ER membrane fluidity and N-glycosylation might also impact the mitochondrial network motility and rescue the AD-associated phenotype. These results prompted us to test whether the changes in motility observed in our model could be associated with impaired cell bioenergetics in AD, and if SPP-treatment could similarly rescue the bioenergetics phenotype of mitochondria in AD-cells.

Mitochondria in AD-Cells Displayed an Inefficient Glycolytic Phenotype Corrected by SPP-Treatment

We used the BBS+ technology (ICDD, France) to assess cell bioenergetics. ATP, Oxygen Consumption Rate (OCR), lactate, NADH and cell viability were recorded in the same cells, without permeabilization. In AD-cells, the amount of ATP was significantly reduced when compared to healthy controls (p=0.0002, n=20) (Figure 2A). This inhibition of ATP production was associated with an increase in OCR, suggesting mitochondrial

membrane uncoupling. It was consistent with the defective complex IV activity previously reported in AD (45). SPP at 0.0002% and 0.005% significantly increased ATP production by 1.24-fold (p=0.0079, n=20) and 1.20-fold (p=0.0221, n=20) respectively (Fig2 A). At 0.005% it also reduced the OCR (p=0.0078, n=20), normalizing the amount of ATP generated per molecule of oxygen consumed (ATP/OCR ratio), a ratio describing cell energy efficiency (Figure 2B). To better understand how ATP was produced in the different experimental conditions, we cultured cells in different media designed to increase the metabolic contribution of the mitochondrial Electron Transfer Chain (ETC). M1 is a medium, which contains all substrates for energy production allowing ATP to be produced by a combination of oxidative phosphorylation, glycolysis, fatty-acid beta-oxidation, ketolysis or the glutamine metabolism pathway (Figure 2C). As previously described [46,47], when glucose supply is reduced (M2), ETC re-engages into ATP production, making it more susceptible to mitochondrial toxicants. When cells were cultured in M2, ETC re-engagement was observed in healthy controls but not in AD-cells, suggesting ETC impairment. Failure to increase OCR after inhibition of glycolysis was not seen in response to SPP 0.005%, which restored ETC engagement to a level comparable to that seen in healthy cells (Figure 2C-E). When both glycolysis and TCA-cycle turning were reduced (M3), ATP production was maintained either through ketolysis or through the glutamine metabolism pathway in AD-cells. SPP-treatment further increased ATP production (Figure 2A). In response to 0.05% SPP, we also observed an increase in activity of the mitochondrial ETC (Figure 2E). SPP effects on cell bioenergetics were not dose-dependent, but rather used threshold progression. At 0.0002% and 0.001%, SPP-induced ATP production mostly relied on fatty-acid beta-oxidation and glycolysis respectively (Figure 2 C,D). When all substrates were available, SPP generated a dose-dependent increase in NADH production, the main substrate for complex I, in AD-cells (supplemental information Figure S1). Our data are consistent with the clinical manifestation of AD, which is characterized by hypometabolism [48,49]. In AD-cells, we found that ATP was mostly produced via the glycolytic pathway, but also that glycolysis was deficient in maintaining a normal ATP level. This result is consistent with the deficient glycolysis hypothesis brought forward to explain sporadic AD as Type 3 diabetes, which was supported by the observation that in oligodendrocytes, genes in the glycolytic pathways were significantly impaired in AD [50-52]. Reduced glucose and oxygen brain metabolism in AD has recently been associated with structural degeneration due to Taupathy and deficit in the ability of brain cells to use glycolytic and ketonic pathways to produce energy [51-53]. Our results demonstrate that fibroblasts derived from AD patients carry similar bioenergetics dysfunction.

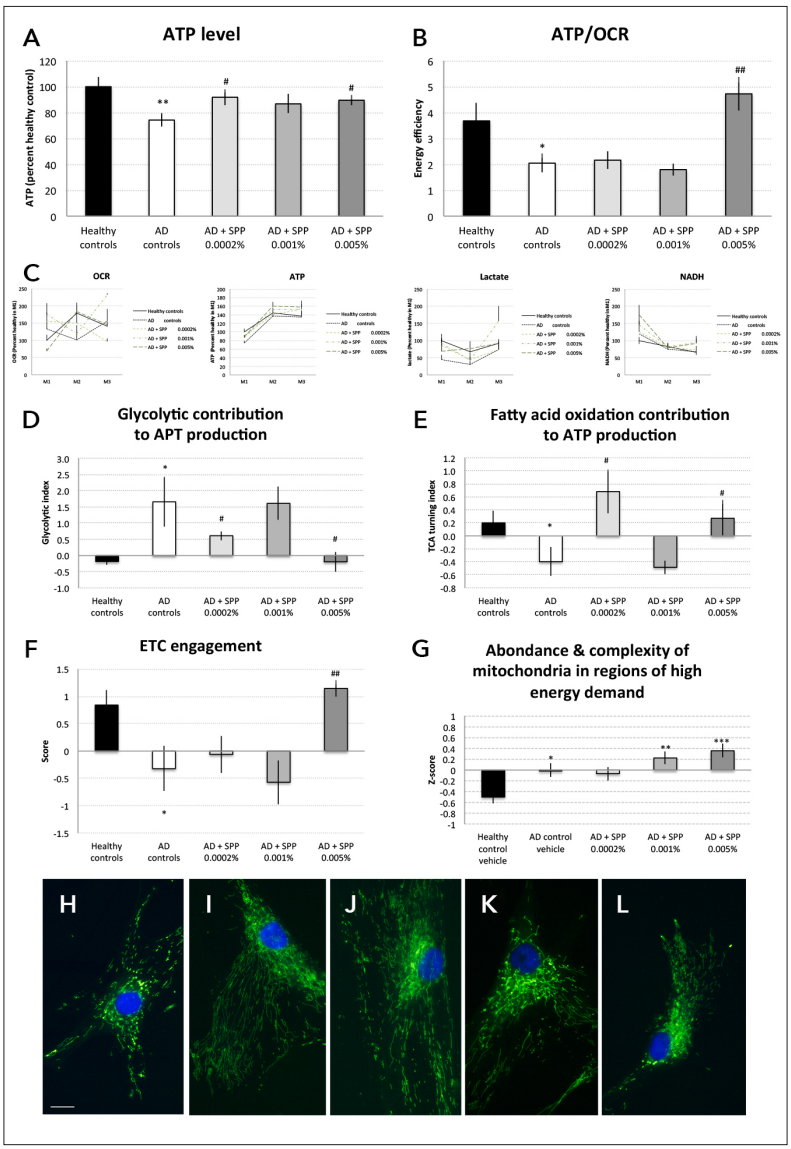

Figure 2: Cell Bioenergetics & Mitochondrial Network Structure at Sites of High-Energy Demand

A: ATP production in cells cultured in non-challenging condition (with all substrates present) expressed as the percent of ATP production in healthy control cells; – B: ATP/OCR ratio representing energy efficiency; – C: Individual outcome measures recorded in live, non-permeabilized cells simultaneously in 3 different media challenging the supply of energy substrate. M1 is a non-challenging medium with all substrate present. M2 is a glucose-free medium, limiting glycolytic contribution to the use of glycogen and gluconeogenesis. M2 is a glucose-free medium containing a carnitine palmitoyltransferase 1 inhibitor, thus limiting both glycolysis and TCA-cycle turning contribution to ATP production. In M3 ATP production is maintained through ketolysis and glutamine metabolic pathway. – D: Glycolytic contribution to ATP production in the different experimental groups; – E: Fatty acid oxidation contribution to ATP production in the different experimental groups, – F: Electron Transfer Chain (ETC) engagement in ATP production in the different experimental groups; – G: Abundance and complexity of the mitochondrial network at sites of high energy demand such as the Peri-Nuclear Area (PNA), the Microtubule Organizing Center (MOC). Analysis done at the cellular level (n=294) – H-L: Mircophotographs representing the increased complexity of the mitochondrial network in PNA and MOC in AD cells, with no effect of SPP treatment. H – Healthy control, I – Untreated AD-cells, J – AD-cells treated with 0.0002% SPP, K – AD-cells treated with 0.001% SPP, L – AD-cells treated with 0.005% SPP. Bar in H represent 10µm. ***p<0.0001, **p<0.001, *p<0.05 indicate significant differences comparing healthy controls to other experimental groups. ###p<0.001, ##p<0.001, #p<0.05 indicate significant differences comparing untreated AD-cells to SPP-treated AD-cells. Error bars are SD in A-F and SEM in G.

Previous reports have suggested a decrease in mtDNA in AD to explain AD-associated bioenergetics impairment (review in [45]). We thus measured this outcome in our model. We found that mtDNA content was not significantly reduced in AD-cells when compared to healthy controls. Treatment with SPP did not modify mtDNA content at any of the tested doses (Supplemental information Fig S2). These results suggested that the observed loss in ATP production was not dependent upon reduced mitochondrial biogenesis, but that it was rather due to reduced bioenergetics efficiency, as seen above. However, these results do not preclude that specific mtDNA halotypes could be present in the AD-cells that are associated with reduced bioenergetics efficiency [45].

We observed an increased complexity in the mitochondrial network in regions of high-energy demand, both in untreated and SPP-treated AD-cells (Figure 2G). SPP-treatment accentuated this phenotype dose-dependently, particularly in regions of high-energy demand (Figure 2G). Others have shown that the complexity of the mitochondrial network may be associated with reduced Complex I activity or compensate for complex IV impairment [54,55]. AD is associated with defects in complex IV. Because SPP restores ATP production and increases energy efficiency, we could speculate that it may either correct the impairment of complex IV or that it may act as a partial inhibitor of complex I. Indeed, partial inhibition of complex I would, paradoxically, improve mitochondrial complex I assembly, increase complex I-linked state 3 respiration and decrease ROS production [56]. It was recently shown to improve Tau-pathology in an AD mouse model [57].

Impact of SPP-Treatment on ER Stress Minimally Contributes to Explaining the Rescue of AD Mitochondrial Motility Phenotype

SPP promoted entanglement of the mitochondrial network, mostly in the PNA, where ATP production is necessary to sustain protein production, folding/traveling and/or degradation [58]. Because protein misfolding is a hallmark of neurodegenerative diseases, comprising both amyloid-beta and Tau proteins in AD, we measured amyloid fibril depositions and Tau hyperphosphorylation in our cell model. Both were significantly increased in AD-cells (Fig 3A-H) by 19-fold ($p \leq 0.0001$, n=268) considering amyloid fibril deposition, and by 4-fold considering Ser235-P Tau expression ($p \leq 0.0001$, n= 360). An effective protein misfolding disorder thus existed in the AD-fibroblast model. Interestingly, response to SPP-treatment resulted in dose-dependent reduction in the deposition of amyloid fibrils in the extracellular space by an average of 0.53-fold ($p \leq 0.0001$, n=268, Fig 3A, C, D). SPP-treatment was slightly more efficient in reducing amyloid fibril deposition at 0.001% (p=0.0006, n=268, Fig 3A). SPP also reduced expression of Ser235-P Tau by an average of 0.52-fold ($p \leq 0.0001$, n=360, Fig 3E, F-H), SPP 0.001% being again the most efficient dose. The expression of Tau was also reduced by 0.44-fold ($p \leq 0.0001$, n=360, Fig 3E, F-H). Again, SPP 0.001% was the most efficient dose with a reduction in Tau expression of 0.30-fold ($p \leq 0.0001$, n=360). The reduced expression of Tau, ser235-P tau and deposition of amyloid fibril may result from the transient shutdown of *de novo* protein synthesis in AD-cells, which could constitute a protective mechanism by which cells control the extent of protein misfolding. Consistent with this interpretation, using click-chemistry, we observed a non-significant 0.79-fold decrease in *de novo* protein synthesis in AD-cells (p=0.7106, n=242, Fig 3I, J-O). An increase in nascent protein synthesis was observed in response to SPP 0.0002% by 1.71-fold (p=0.0117, n=242, Fig 3I, M) and to SPP 0.005% by 2.00-fold (p=0.0008, n=242, Fig 3I, O) compared to untreated AD-cells.

The Protein Kinase RNA-like Endoplasmic Reticulum Kinase (PERK) pathway inhibits general mRNA translation, decreasing nascent protein synthesis thus reducing the ER load [59]. PERK is one of the major Unfolded Protein Response (UPR) pathways that detect protein-folding imbalances during ER-stress in AD [60,61]. As a result of PERK activation, the level of phosphorylated Eukaryotic Initiation Factor 2 alpha (eIF2α) is markedly elevated, resulting in the inhibition of global protein synthesis, while selectively activating the translation of Activating Transcription Factor 4, C/EBP homologous protein and BACE [62-64]. Because SPP is an isoprenoid precursor of dolichol, it may modulate protein glycosylation and treatment of AD cultures with SPP could reduce ER stress to enhance protein synthesis [65]. We thus measured eIF2α and Ser51-P eIF2α expression in our experimental conditions. SPP significantly reduced eIF2α expression in a dose dependent manner, compared to untreated AD-cells (p=0.0094, n=40, Fig 3 P-R). The most potent dose was 0.005%, where we observed a 0.63-fold decrease in eIF2α expression (p=0.0180, n=40, Fig 3P-R). We found no increase in Ser51-P eIF2α expression in AD-cells compared to healthy controls (p=0.2189, n=40, Fig 3 Q-R). Similarly, Ser51-P eIF2α expression was not significantly reduced by SPP-treatment in AD-cells, despite an average 0.67-fold decrease in Ser51-P eIF2α expression (Fig 3Q-R). Hence, SPP reduced ER-stress by weakly antagonizing the PERK signaling pathway. The decrease in eIF2α and Ser51-P eIF2α expression was consistent with the increase in nascent protein synthesis observed in our model. As

Citation: Giorgio Dell'Acqua, Tony McFadden, Beatrice Blanc, Romain MJ Lasseur, Nicolas Brouilly, et al. (2025) Plant Polyprenols Disrupt the IP3R-GRP75-VDAC-MCU Axis to Restore Mitochondrial Motility Defects Associated with Alzheimer's Disease. Journal of Alzheimer's Disease & Reports. SRC/JADR-111.
DOI: doi.org/10.47363/JADR/2025(2)110

reported by others, reduction in ER-stress is also consistent with the reduction in amyloid fibrillation that we observed [66]. This data, ruled out the possible impact of PERK signaling on the UPR pathway to explain the phenotypic changes observed in response to SPP in the mitochondrial network. It opened however, the possibility that they could at least partially be due to a role of PERK in tethering ER membrane and mitochondrial membrane at MAMs, a function that does not require PERK enzyme activity [67-69].

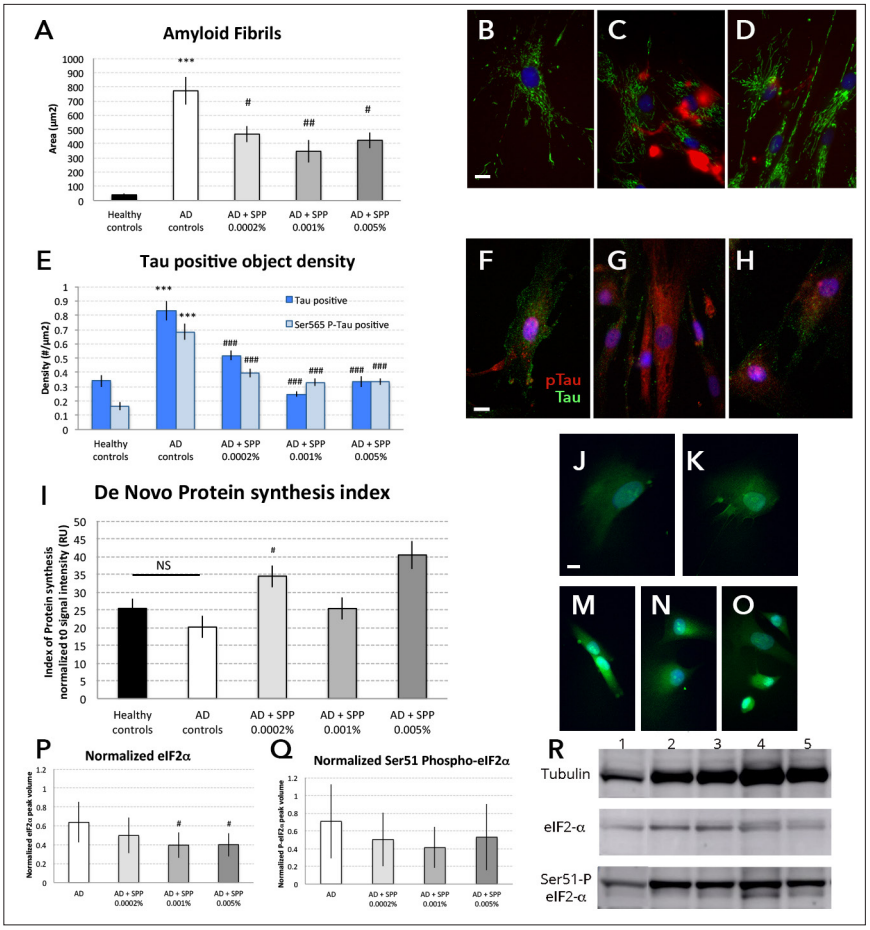

Figure 3: Protein Misfolding & ER Stress

A: Quantification of amyloid fibril deposition in the extracellular space, analysis done at the cellular level using Slidebook software (n=268)– B-D: microphotographs representative of the experimental conditions studied, B- Healthy control, C- untreated AD-cells, D- AD-cells treated with SPP 0.001%. Bar in B represents 10µm. – E: Quantification of Tau and P-Tau expression in the different experimental conditions, analysis done at the cellular level using Slidebook software (n=360)– F-H: microphotographs representative of the experimental conditions studied, F- Healthy control, G- untreated AD-cells, H- AD-cells treated with SPP 0.001%. Bar in F represents 10µm. I: Quantification of click-chemistry signal measuring *de novo* protein synthesis in a methionine free medium, analysis done at the cellular level using Slidebook software (n=251). J-O: microphotographs representative of the experimental conditions studied, J- Healthy control, K- untreated AD-cells, M- AD-cells treated with SPP 0.0002%, N- AD-cells treated with SPP 0.001%, O- AD-cells treated with SPP 0.005%. Bar in J represents 10µm. P-Q: Quantification of the expression of eIF2α (P) and Ser51-P eIF2α (Q), R Representative western blot (3 independent experiments performed and quantified).

###p<0.001, ##p<0.001, #p<0.05 indicate significant differences comparing untreated AD-cells to SPP-treated AD-cells. Error bars are SEM in A, E and I and SD on P and Q.

SPP Mediated the Disruption of the IP3R-GRP75-VDAC-MCU Axis at MAMs

Impaired MAM signaling has wide-ranging effects in many diseases, such as obesity, diabetes, and neurodegenerative disorders, modulating Ca^{2+} signaling, lipid metabolism, mitochondrial function, ER stress responses and inflammation [70]. We thus explored how MAMs were affected in the AD-cell model used. MAMs are linked to intracellular trafficking of mitochondria and ER. Modulation of MAM quality or signaling could explain the motility behavior observed in AD-cells and offer a biological process to further explore the mechanism of action of SPP-treatment.

We used a proximity ligation assay to monitor physical contact points at MAMs. We chose to monitor interactions between the Sarco/endoplasmic reticulum (SR/ER) Ca^{2+} ATPase pump (SERCA), situated on ER, with the mitochondrial protein Glucose-Regulated Protein 75 (GRP75) Situated in the mitochondrial iPR3-VDAC-GPR75 complex. SERCA is one of the main proteins controlling calcium storage in the ER. GRP75, a mitochondrial matrix chaperone, is involved in strengthening mitochondria-ER crosstalk through the complex iPR3-VDAC-GPR75, controlling calcium fluxes in and out of the mitochondria.

Citation: Giorgio Dell'Acqua, Tony McFadden, Beatrice Blanc, Romain MJ Lasseur, Nicolas Brouilly, et al. (2025) Plant Polyprenols Disrupt the IP3R-GRP75-VDAC-MCU Axis to Restore Mitochondrial Motility Defects Associated with Alzheimer's Disease. Journal of Alzheimer's Disease & Reports. SRC/JADR-111.
DOI: doi.org/10.47363/JADR/2025(2)110

We observed a significant 3.50-fold increase in ER-mitochondria contact points at MAMs in AD-cells compared to healthy control cells ($p \leq 0.0001$, n=364, Fig 4B-D) (Figure 4A). In response to SPP-treatment, the number of ER-mitochondria contact points at MAMs was reduced in a dose-dependent manner ($p \leq 0.0001$, n=364, Fig 4B). All doses used were efficient in reducing the number of iPR3-VDAC-GPR75/SERCA interactions at MAMs. SPP 0.001% was the most efficient dose, with a decrease of 0.64-fold ($p \leq 0.0001$, n=364, Fig 4A, 4D), which plateaued thereafter. Inhibiting the iP3R1–GRP75–VDAC1 complex can prevent calcium transfer from the ER to the mitochondria and attenuate mitochondrial calcium overload, while contributing to a normalization of intracellular calcium concentration [71]. Such a mechanism may also contribute to the normalization of ATP production in AD-cells treated with SPP.

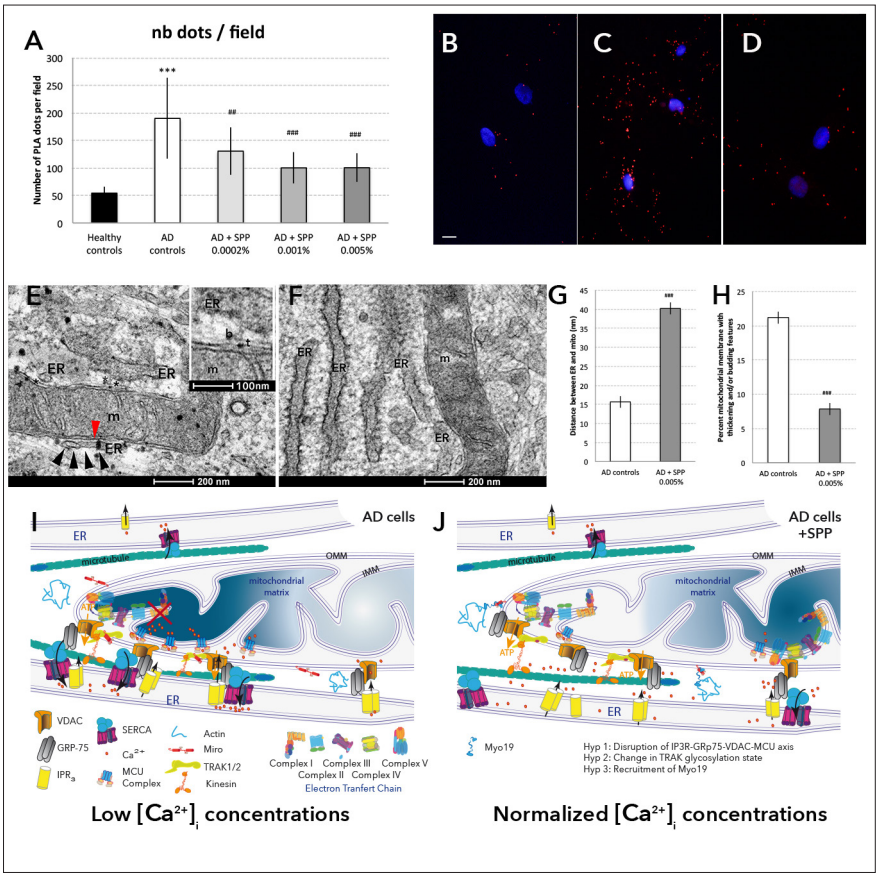

Figure 4: ER-Mitochondria Associated Membrane are Targeted by AD and SPP-Treatment

A: Quantification of MAMs identified by the proximity of SERCA to the GRP75-VDAC-MCU axis using proximity ligation assay, analysis done at the cellular level using Slidebook software (Analysis done at the cellular level, n=364, error bars are SD)– B-D representative microphotographs of the experimental conditions studied, B- Healthy control, C- untreated AD-cells, D- AD-cells treated with SPP 0.005%. Bar in BB is 10µm. E Electron transmission microcopy microphotograph without staining was performed in untreated AD-cells (E) and in 0.005% SPP-treated AD-cells, to confirm the impact of treatment on occurrence of putative MAMs without antibody staining. – G: Quantification of MAMs in electron microphotographs using distance between ER and mitochondrial membrane below 30nm as an indication for the presence of putative MAMs. (Analysis done in 3 independent replicates, n= 293 measurements). – H: Quantification of the occurrence of either membrane thickening or budding at putative MAMs. (Analysis done in 3 independent replicates, n= 293 measurements, error bars are SEM). ***$p<0.0001$, **$p<0.001$, *$p<0.05$ indicate significant differences comparing healthy controls to other experimental groups. ###$p<0.001$, ##$p<0.001$, #$p<0.05$ indicate significant differences comparing untreated AD-cells to SPP-treated AD-cells.

We performed transmission electron microscopy comparing the AD-control and AD-cells treated with 0.005% SPP (Fig 4E-H). We observed a significant 2.56-fold increase in the average distance between the smooth or rougher ER and mitochondria in SPP-treated versus untreated AD-cells ($p \leq 0.0001$, n= 293, Fig3G). We also observed a significant 0.37-fold decrease in features associated with membrane contact such as budding or thickening in SPP-treated versus untreated AD-cells ($p \leq 0.0001$, n= 293, Fig3H). Finally, a Chi square test of independence was performed to examine the relation between treatment groups and occurrence of MAMs as defined by an unsupervised ranking of the distances between ER and mitochondria below 30nm in untreated and 0.005% SPP-treated AD-cells. The relation between treatment groups and occurrence of putative MAMs was significant, χ^2 (1, N=293) = 87.144, p = ≤0.0001. Untreated AD-cells were more likely to display an increased number of putative MAM than SPP-treated AD-cell.

Explaining the Biological Basis for AD Mitochondrial Phenotype

Our data suggest that, in AD-cells, increased contact points at MAMs involving the VDAC-GRP75-IP3R complex and SERCA are likely to generate locally reduced cytosolic free calcium concentrations ($[Ca^{2+}]i$), increasing calcium storage in both the mitochondria and more modestly in the ER (Model in Fig 4I). Mitochondrial calcium overload is thought to reduce ATP production, possibly adding to the observed impaired efficiency in bioenergetics in AD-cells [72]. It has also been shown that $[Ca^{2+}]_i$ regulate mitochondrial movements. In neurons, elevation of $[Ca^{2+}]_i$ slows both the anterograde and the retrograde movement of mitochondria [73-75]. Conversely locally reduced $[Ca^{2+}]_i$ may provide a rationale for the lack of mitochondrial docking observed in this study. While resting, $[Ca^{2+}]_i$ are reported to be in the range of ~0.1 µM [76]. Studies have shown that ~0.4µM of $[Ca^{2+}]_i$ is needed to cause 50% reduction in mitochondrial movement and complete arrest occurs at low micromolar concentrations [41-43]. Low $[Ca^{2+}]_i$ is a feature of AD, found both in neuron and fibroblasts models, indirectly confirming our model [77,78].

Calcium binding proteins containing EF-hands such as Miro 1/2 and Mitochondrial Calcium Uptake (MICU 1/2/3), which interacts with the Mitochondrial Calcium Uniporter (MCU), are likely to be affected by the local changes in $[Ca^{2+}]_i$. Miro1/2 may not be the sole target(s) for the observed mitochondrial phenotype in AD-cells. The signaling of other mitochondrial EF-hands containing proteins could also be affected. They include the transmembrane protein 1 (LETM1), the glycerol-3-phosphate dehydrogenase (mtGPDH), the Mitochondrial Glutamate/Aspartate Carrier (AGC1), the calcium binding mitochondrial carrier protein SCaMC1/2/3 (a family of mitochondrial phosphate and other solute carrier), and the S100 calcium binding protein A1 (S100A1). These proteins' function may impact mitochondrial energy metabolism, particularly the NADH metabolic process, mitochondrial shape and/or the transport of metabolites, nucleotides and cofactors (not shown in our model) [79, 80].

We favor the possible role of Miro 1/2 proteins located at MAMs, which are known to indirectly bind microtubules and actin filaments participating in the regulation of mitochondrial movements and distribution in the cell [81]. Using various knockout methodologies, others have shown that Miro loss of function resulted in defects in mitochondrial cell distribution and motility. It notably increased docking in retrograde mitochondrial movements. These defects were sufficient to cause motor neurons developmental defects [82,83].

The data presented above demonstrate a global deficit in the docking of mitochondria in AD-cells compared to healthy age and gender-matched controls. They more specifically highlight a mitochondrial sub-population, the "Sentry" mitochondrion, representing about 15% of the mitochondrial network. This subpopulation lacks the capability to dock thus traveling longer distances without being able to arrest where mitochondrial function is required. This observation points to a possible gain of function in Miro 1/2, which interaction with the Milton homologs, TRACK1 or TRACK2, is dependent upon the glycosylation state of these proteins. By enhancing motor activity and mitochondria transport along microtubules it would explain the mitochondrial phenotype observed [83, 84].

Modeling Putative Biological Bases for the SPP-Mediated Rescue of the Ad-Mitochondrial Phenotype

An hypothetical model is presented in Fig 4 J representing the putative biological processes by which SPP-treatment normalized mitochondrial bioenergetics and MAMs formation/signaling in AD-cells, restoring docking capabilities in the Sentry mitochondrial sub-population. Because SPP mediated the disruption of the IP3R-GRP75-VDAC-MCU axis at MAMs:

- It may induce a calcium leak from the ER through IP3R, thus locally increasing $[Ca^{2+}]i$, modulating the signaling of calcium sensing proteins such as MICU to limit mitochondrial calcium overload.
- It may also modulate the activity of other mitochondrial calcium sensing proteins such as the mitochondrial carriers for aspartate/glutamate, which modulate the malate-aspartate NADH shuttle, consistent with the dose-dependent increase in NADH observed in response to SPP [79].
- Miro 1 or Miro 2 could also be targeted by SPP. Indeed, Ca^{2+} binding to Miro triggers the dissociation of either Miro/TRAK or TRAK/KIF5 interaction, thereby uncoupling KIF5 from the mitochondrial surface [44, 85].
- Furthermore, SPP could target TRAK1/2, which glycosylation state has been reported to control interactions with Miro and conferring glucose sensitivity to mitochondrial motility [39].
- By limiting Miro/TRAK or TRAK/KIF5 interactions, SPP may also provide a signal for the recruitment of Myo19 to Miro to increase interactions of mitochondria with the actin filaments, thus increasing stability and docking of mitochondria.

Therefore, the disruption of the IP3R-GRP75-VDAC-MCU axis by SPP may provide a rationale to explain the modulation of mitochondrial movements by SPP in AD-cells. The role of SPP at MAMs may also explain its impact on amyloid deposition. Amyloid deposition was reported to be correlated with increased MAMs signaling [86]. Others have described increased MAMs contact points in presenilin-mutant cells and in fibroblasts from patients with both familial and sporadic AD [87]. In these studies, increased MAMs contact points were correlated with increased cholesteryl ester and phospholipid synthesis. It is interesting to note that dolichol participates in the biosynthesis of cholesterol and phospholipids and N-glycosylation in the endoplasmic reticulum, thus providing a testable hypothesis for the impact of SPP on amyloid fibrillation [88].

Conclusion

SPP action at MAMs may thus explain most of the biological effects observed in our model. These suggested mechanisms are crucial in the context of neurodegenerative diseases and aging. The modulation of the SERCA2/IPR3-GRP75-VDAC-MCU axis by AD pathophysiology could be reversed by SPP-treatment and could allow mitochondrial arrest as soon as the $[Ca^{2+}]i$ is increased. The putative impact of SPP on O-GlcNAc transferase to modify TRAK glycosylation state provides a selective and glucose-dependent mechanism for arrest of mitochondrial motility. Alternatively, SPP may also modulate the lipid transport proteins to maintain membrane homeostasis in the ER. There, Miro could also mediate SPP's action as it also promotes lipid transfer at MAMs and between ER–peroxisome contact sites [89,90].

Our results therefore provide a rationale for the use of SPP in improving resilience of the brain during aging, delaying cognitive impairment or in the mitigation of cognitive loss associated with AD in the elderly population.

Acknowledgments
We thank Pauline Picamal and Clotilde Biscarrat for technical assistance. The electron microscopy experiments were carried out on the IBDM Electron Microscopy Facility, member of the National Infrastructure France-BioImaging (ANR-24-INBS-0005 FBI BIOGEN). We also thank Dr. Soultanov for critical review of the paper prior to its submission.

Funding Statement
This work was supported by Juvesen Pty Ltd.

Declaration of Conflicting Interests
The author(s) declared the following potential conflicts of interest with respect to the research, authorship, and/or publication of this article: TM is the founder of Juvesen Pty Ltd and holds equity. ICDD received research funding from Juvesen Pty Ltd to perform this work. The remaining authors declare no competing interests.

Author Contributions
NAC and GDA conceptualized and designed research; GDA and TMcF contributed new reagent / analytical tools, BB, PP and RMJL performed research; NB performed EM experiments, BB and NAC analyzed data; and NAC wrote the paper. All authors approved the submitted version.

Significance Statement
Aging is the leading risk factor for AD. It represents a significant health burden in high-income countries, where the proportion of people above 65yo is increasing. Brain aging and neurodegenerative diseases involve mitochondria- and ER-mitochondria contact-related $[Ca^{2+}]$i regulatory defects. Defective $[Ca^{2+}]$i transfer to mitochondria disturbs oxidative phosphorylation, thereby increasing ROS production leading to cellular damage, observed in both aging and neurodegenerative diseases. Up-regulation of $[Ca^{2+}]$i levels both initiate and accelerate several AD features, from amyloid deposition to synapse loss. Here we show that standardized plant polyprenols disrupted the IP3R-GRP75-VDAC-MCU axis, restored mitochondrial docking and increased mitochondrial bioenergetics. This observation was associated with reduced amyloid fibrillation and Tau hyperphosphorylation suggesting it may be an attractive candidate for modifying pathological brain aging.

References

1. Compagnone NA, Biscarrat C (2015) WO2015040214A1, Method of screening for compounds useful in the treatment of Alzheimer disease.
2. Compagnone NA (2010) WO2009034094A1, Method to predict toxicity using the analysis of dynamic organelle behaviour.
3. Tilokani LS, Nagashima V, Paupe J Prudent (2018) Mitochondrial dynamics: overview of molecular mechanisms. Essays Biochem 62: 341-360.
4. Chan DC (2012) Fusion and fission: interlinked processes critical for mitochondrial health. Annu. Rev. Genet 46: 265-287.
5. Youle RJ, van der Bliek AM (2012) Mitochondrial fission, fusion, and stress. Science 337: 1062-1065.
6. Saxton WM, Hollenbeck PJ (2012) The axonal transport of mitochondria. J Cell Sci 125: 2095-2104.
7. Van der Bliek AM, Shen Q, Kawajiri S (2013) Mechanisms of mitochondrial fission and fusion. Cold Spring Harb Perspect Biol 5: 011072.
8. Melser S, Lavie J, Bénard G (2015) Mitochondrial degradation and energy metabolism. Biochimica et Biophysica Acta (BBA) - Molecular Cell Research 1853: 2812-2821.
9. Schwarz N, Leube RE (2016) Intermediate Filaments as Organizers of Cellular Space: How They Affect Mitochondrial Structure and Function. Cells 5: 30.
10. Baker N, Patel J, Khacho M (2019) Linking mitochondrial dynamics, cristae remodeling and supercomplex formation: How mitochondrial structure can regulate bioenergetics. Mitochondrion 49: 259-268.
11. Xinglong Wang, Bo Su, Hyoung-gon Lee, Xinyi Li, George Perry, et al. (2009) Impaired Balance of Mitochondrial Fission and Fusion in Alzheimer's Disease. J Neurosci 29: 9090-9103.
12. Patricia Martín Maestro, Ricardo Gargini, Esther García, George Perry, Jesús Avila, et al. (2017) Slower Dynamics and Aged Mitochondria in Sporadic Alzheimer's Disease. Oxid Med Cell Longev 2017: 9302761.
13. Chan DC (2020) Mitochondrial Dynamics and Its Involvement in Disease. Annu Rev Pathol Mech Dis 15: 235-259.
14. Rambold AS, Kostelecky B, Elia N, Lippincott-Schwartz J (2011) Tubular network formation protects mitochondria from autophagosomal degradation during nutrient starvation. Proceedings of the National Academy of Sciences 108: 10190-10195.
15. Bulthuis EP, Adjobo-Hermans MJW, Willems PHGM, Koopman WJH (2019) Mitochondrial Morphofunction in Mammalian Cells. Antioxid Redox Signal 30: 2066-2109.
16. Yang L, Wang C, Ye J, Li H (2011) Hepatoprotective effects of polyprenols from Ginkgo biloba L. leaves on CCl4-induced hepatotoxicity in rats. Fitoterapia 82: 834-840.
17. Marina Y Khodanovich, Anna O Pishchelko, Valentina Y Glazacheva, Edgar S Pan, Elena P Krutenkova, et al. (2019) Plant polyprenols reduce demyelination and recover impaired oligodendrogenesis and neurogenesis in the cuprizone murine model of multiple sclerosis. Phytotherapy Research 33: 1363-1373.
18. Fedotova J, Soultanov V, Nikitina T, Roschin V, Ordayn N (2012) Ropren (®) is a polyprenol preparation from coniferous plants that ameliorates cognitive deficiency in a rat model of beta-amyloid peptide-(25-35)-induced amnesia. Phytomedicine 19: 451-456.
19. Swiezewska E, Danikiewicz W (2005) Polyisoprenoids: structure, biosynthesis and function. Prog Lipid Res 44: 235-258.
20. Vincent Cantagrel, Dirk J Lefeber, Bobby G Ng, Ziqiang Guan, Jennifer L Silhavy, et al. (2010) SRD5A3 is required for converting polyprenol to dolichol and is mutated in a congenital glycosylation disorder. Cell 142: 203-217.
21. Edlund C, Söderberg M, Kristensson K, Dallner G (1992) Ubiquinone, dolichol, and cholesterol metabolism in aging and Alzheimer's disease. Biochem Cell Biol 70: 422-428.
22. Pullarkat RK, Reha H (1982) Accumulation of dolichols in brains of elderly. J Biol Chem 257: 5991-5993.
23. Parentini I, Cavallini G, Donati A, Gori Z, Bergamini E (2005) Accumulation of dolichol in older tissues satisfies the proposed criteria to be qualified a biomarker of aging. J Gerontol A Biol Sci Med Sci 60: 39-43.
24. Yu L, Zhiguang Huo, Jingyun Yang, Helena Palma-Gudiel, Patricia A, et al. (2021) Human Brain and Blood N-Glycome Profiling in Alzheimer's Disease and Alzheimer's Disease-Related Dementias. Front Aging Neurosci 13: 765259.
25. Conroy LR, Hawkinson TR, Young LEA, Gentry MS, Sun RC (2021) Emerging roles of N-linked glycosylation in brain physiology and disorders. Trends in Endocrinology & Metabolism 32: 980-993.

26. Ramon C Sun, Lyndsay EA Young, Ronald C Bruntz, Kia H Markussen, Zhengqiu Zhou, et al. (2021) Brain glycogen serves as a critical glucosamine cache required for protein glycosylation. Cell Metabolism 33: 1404-1417.
27. Tan EP, Steven R McGreal, Stefan Graw, Robert Tessman, Scott J Koppel, et al. (2017) Sustained O-GlcNAcylation reprograms mitochondrial function to regulate energy metabolism. J Biol Chem 292: 14940-14962.
28. Tan EP, Maria T Villar, Lezi E, Jianghua Lu, J Eva Selfridge, et al. (2014) Altering O-linked β-N-acetylglucosamine cycling disrupts mitochondrial function. J Biol Chem 289: 14719-14730.
29. Curti D, Rognoni F, Gasparini L, Cattaneo A, Paolillo M, et al. (1997) Oxidative metabolism in cultured fibroblasts derived from sporadic Alzheimer's Disease (AD) patients. Neurosci Lett 236: 13-16.
30. Chiara P Zoia, Elena Tagliabue, Valeria Isella, Barbara Begni, Lorenzo Fumagalli, et al. (2005) Fibroblast glutamate transport in aging and in AD: correlations with disease severity. Neurobiol Aging 26: 825-832.
31. Martín-Maestro P, Ricardo Gargini, Andrew A Sproul, Esther García, Luis C Antón, et al. (2017) Mitophagy Failure in Fibroblasts and iPSC-Derived Neurons of Alzheimer's Disease-Associated Presenilin 1 Mutation. Frontiers in Molecular Neuroscience 10: 291.
32. Pérez MJ, Ponce DP, Aranguiz A, Behrens MI, Quintanilla RA (2018) Mitochondrial permeability transition pore contributes to mitochondrial dysfunction in fibroblasts of patients with sporadic Alzheimer's disease. Redox Biol 19: 290-300.
33. Pérez MJ, Ponce DP, Osorio-Fuentealba C, Behrens MI, Quintanilla RA (2017) Mitochondrial Bioenergetics Is Altered in Fibroblasts from Patients with Sporadic Alzheimer's Disease. Frontiers in Neuroscience 11: 553.
34. Calkins MJ, Manczak M, Mao P, Shirendeb U, Reddy PH (2011) Impaired mitochondrial biogenesis, defective axonal transport of mitochondria, abnormal mitochondrial dynamics and synaptic degeneration in a mouse model of Alzheimer's disease. Human Molecular Genetics 20: 4515-4529.
35. Heng Du, Lan Guo, Shiqiang Yan, Alexander A Sosunov, Guy M McKhann, et al. (2010) Early deficits in synaptic mitochondria in an Alzheimer's disease mouse model. Proceedings of the National Academy of Sciences 107: 18670-18675.
36. John Z Cavendish, Saumyendra N Sarkar, Mark A Colantonio, Dominic D Quintana, Nadia Ahmed, et al. (2019) Mitochondrial Movement and Number Deficits in Embryonic Cortical Neurons from 3xTg-AD Mice. J Alzheimers Dis 70: 139-151.
37. Flannery PJ, Trushina E (2019) Mitochondrial Dynamics and Transport in Alzheimer's Disease. Mol Cell Neurosci 98: 109-120.
38. Matsumoto N, Ikuma Hori, Masashi K Kajita, Tomoya Murase, Wataru Nakamura, et al. (2022) Intermitochondrial signaling regulates the uniform distribution of stationary mitochondria in axons. Molecular and Cellular Neuroscience 119: 103704.
39. Pekkurnaz G, Trinidad JC, Wang X, Kong D, Schwarz TL (2014) Glucose Regulates Mitochondrial Motility via Milton Modification by O-GlcNAc Transferase. Cell 158: 54-68.
40. Himanish Basu, Gulcin Pekkurnaz, Jill Falk, Wei Wei, Morven Chin, et al. (2021) FHL2 anchors mitochondria to actin and adapts mitochondrial dynamics to glucose supply. J Cell Biol 220: e201912077.
41. Masao Saotome, Dzhamilja Safiulina, György Szabadkai, Sudipto Das, Asa Fransson, et al. (2008) Bidirectional Ca^{2+}-dependent control of mitochondrial dynamics by the Miro GTPase. Proc Natl Acad Sci USA 105: 20728-20733.
42. Jackson JG, Robinson MB (2015) Reciprocal Regulation of Mitochondrial Dynamics and Calcium Signaling in Astrocyte Processes. J Neurosci 35: 15199-15213.
43. Yi M, Weaver D, Hajnóczky G (2004) Control of mitochondrial motility and distribution by the calcium signal: a homeostatic circuit. Journal of Cell Biology 167: 661-672.
44. Andrew F Macaskill, Johanne E Rinholm, Alison E Twelvetrees, I Lorena Arancibia-Carcamo, James Muir, et al. (2009) Miro1 Is a Calcium Sensor for Glutamate Receptor-Dependent Localization of Mitochondria at Synapses. Neuron 61: 541-555.
45. Giacomo Monzio Compagnoni, Alessio Di Fonzo, Stefania Corti, Giacomo P Comi, Nereo Bresolin, et al. (2020) The Role of Mitochondria in Neurodegenerative Diseases: the Lesson from Alzheimer's Disease and Parkinson's Disease. Mol Neurobiol 57: 2959-2980.
46. Crabtree HG (1929) Observations on the carbohydrate metabolism of tumours. Biochem. J 23: 536-545.
47. Marroquin LD, Hynes J, Dykens JA, Jamieson JD, Will Y (2007) Circumventing the Crabtree effect: replacing media glucose with galactose increases susceptibility of HepG2 cells to mitochondrial toxicants. Toxicol Sci 97: 539-547.
48. Lisa Mosconi, Valentina Berti, Lidia Glodzik, Alberto Pupi, Susan De Santi, et al. (2010) Pre-Clinical Detection of Alzheimer's Disease Using FDG-PET, with or without Amyloid Imaging. J Alzheimers Dis 20: 843-854.
49. Levin F, Daniel Ferreira, Catharina Lange, Martin Dyrba, Eric Westman, et al. (2021) Data-driven FDG-PET subtypes of Alzheimer's disease-related neurodegeneration. Alzheimer's Research & Therapy 13: 49.
50. Dela Monte SM, Wands JR (2008) Alzheimer's Disease Is Type 3 Diabetes-Evidence Reviewed. J Diabetes Sci Technol 2: 1101-1113.
51. Saito ER, Justin B Miller, Oscar Harari, Carlos Cruchaga, Kathie A Mihindukulasuriya, et al. (2021) Alzheimer's Disease Alters Oligodendrocytic Glycolytic and Ketolytic Gene Expression. Alzheimer's & Dementia 17: 1474-1486.
52. González A, Calfío C, Churruca M, Maccioni RB (2022) Glucose Metabolism and Ad: Evidence for a Potential Diabetes Type 3. Alzheimer's Research & Therapy 14: 56.
53. Strom A, Leonardo Iaccarino, Lauren Edwards, Orit H Lesman-Segev, David N Soleimani-Meigooni, et al. (2022) Cortical Hypometabolism Reflects Local Atrophy and Tau Pathology in Symptomatic Alzheimer's Disease. Brain 145: 713-728.
54. Koopman WJH, Henk-Jan Visch, Sjoerd Verkaart, Jan AM Smeitink, Lambertus WPJ van den Heuvel, et al. (2005) Mitochondrial Network Complexity and Pathological Decrease In Complex I Activity Are Tightly Correlated in Isolated Human Complex I Deficiency. American Journal of Physiology-Cell Physiology 289: C881-C890.
55. Rolland SG, Elisa Motori, Nadin Memar, Jürgen Hench, Stephan Frank, et al. (2013) Impaired Complex Iv Activity in Response to Loss of Lrpprc Function can be Compensated by Mitochondrial Hyperfusion. Proc Natl Acad Sci USA 110: E2967-E2976.
56. Miwa S, Howsun Jow, Karen Baty, Amy Johnson, Rafal Czapiewski, et al. (2014) Low Abundance of the Matrix Arm of Complex I In Mitochondria Predicts Longevity in Mice. Nat Commun 5: 3837.
57. Stojakovic A, Su-Youne Chang, Jarred Nesbitt, Nicholas P

Pichurin, Mark A Ostroot, et al. (2021) Partial Inhibition of Mitochondrial Complex I Reduces Tau Pathology and Improves Energy Homeostasis and Synaptic Function In 3xtg-Ad Mice. J Alzheimers Dis 79: 335-353.

58. Arrieta A, Blackwood EA, Stauffer WT, Glembotski CC (2020) Integrating Er and Mitochondrial Proteostasis in the Healthy and Diseased Heart. Front Cardiovasc Med 6: 193.
59. Dever TE (2002) Gene-Specific Regulation by General Translation Factors. Cell 108: 545-556.
60. Wang P, Li J, Sha B (2016) The Er Stress Sensor Perk Luminal Domain Functions as A Molecular Chaperone to Interact with Misfolded Proteins. Acta Crystallogr D Struct Biol 72: 1290-1297.
61. Wang P, Li J, Tao J, Sha B (2018) The Luminal Domain of the Er Stress Sensor Protein Perk Binds Misfolded Proteins and Thereby Triggers Perk Oligomerization. J Biol Chem 293: 4110-4121.
62. Donnelly N, Gorman AM, Gupta S, Samali A (2013) The Eif2α Kinases: Their Structures and Functions. Cell Mol Life Sci 70: 3493-3511.
63. Han J, Sung Hoon Back, Junguk Hur, Yu-Hsuan Lin, Robert Gildersleeve, et al. (2013) Er-Stress-Induced Transcriptional Regulation Increases Protein Synthesis Leading to Cell Death. Nat Cell Biol 15: 481-490.
64. O'Connor T, Katherine R Sadleir, Erika Maus, Rodney A Velliquette, Jie Zhao, et al. (2008) Phosphorylation of the Translation Initiation Factor eIF2α Increases BACE1 Levels and Promotes Amyloidogenesis. Neuron 60: 988-1009.
65. De Giorgi M, Kelsey E Jarrett, Jason C Burton, Alexandria M Doerfler, Ayrea Hurley, et al. (2020) Depletion of Essential Isoprenoids and Er Stress Induction Following Acute Liver-Specific Deletion of Hmg-Coa Reductase. J Lipid Res 61: 1675-1686.
66. Wu Y, Qingjie Chen, Bing Wen, Ninghua Wu, Benhong He, et al. (2021) Berberine Reduces Aβ42 Deposition and Tau Hyperphosphorylation Via Ameliorating Endoplasmic Reticulum Stress. Front Pharmacol 12: 640758.
67. Lebeau J, Jaclyn M Saunders, Vivian W R Moraes, Aparajita Madhavan, Nicole Madrazo, et al. (2018) The Perk Arm of the Unfolded Protein Response Regulates Mitochondrial Morphology During Acute Endoplasmic Reticulum Stress. Cell Rep 22: 2827-2836.
68. Sciarretta S, Kitsis RN, Sadoshima J (2021) Mitochondrial Dysfunction and Cardiovascular Diseases (Frontiers Media SA, 2021) 8. https://www.frontiersin.org/journals/cardiovascular-medicine/articles/10.3389/fcvm.2021.645986/full.
69. Verfaillie T, Rubio N, Garg AD, Bultynck G, Rizzuto R, et al. (2012) PERK is Required at the ER-mitochondrial Contact Sites to Convey Apoptosis After ROS-Based ER Stress. Cell Death Differ 11: 1880-1891.
70. Paillusson S, Radu Stoica, Patricia Gomez-Seaga, Dawn HW Lau, Sarah Mueller, et al. (2016) There's Something Wrong with my MAM; the ER-Mitochondria Axis and Neurodegenerative Diseases. Trends Neurosci 3: 146-157.
71. Xu H, Han Xu, Na Guan, Ya-Li Ren, Qi-Jiao Wei, et al. (2018) IP3R-Grp75-VDAC1-MCU Calcium Regulation Axis Antagonists Protect Podocytes from Apoptosis and Decrease Proteinuria in an Adriamycin Nephropathy Rat Model. BMC Nephrol 19: 140.
72. Strubbe-Rivera JO, Jasiel O Strubbe-Rivera, Jiahui Chen, Benjamin A West, Kristin N Parent, et al. (2021) Modeling the Effects of Calcium Overload on Mitochondrial Ultrastructural Remodeling. Appl Sci (Basel) 11: 2071.
73. Rintoul GL, Filiano AJ, Brocard JB, Kress GJ, Reynolds IJ, et al. (2003) Glutamate Decreases Mitochondrial Size and Movement in Primary Forebrain Neurons. J. Neurosci 23: 7881-7888.
74. Chang KT, Niescier RF, Min KT (2011) Mitochondrial matrix Ca^{2+} as an intrinsic signal regulating mitochondrial motility in axons. Proceedings of the National Academy of Sciences 108: 15456-15461.
75. Szabadkai G, Simoni Am, Bianchi K, Stefani D De, Leo S et al. (2006) Mitochondrial dynamics and Ca^{2+} signaling. Biochim Biophys Acta 1763: 442-449.
76. Malgaroli A, Milani M, Melodies J, Pozzan T (1987) Fura-2 measurement of cytosolic free Ca^{2+} in monolayers and suspensions of various types of animal cells. J Cell Biol 105: 2145-2155.
77. Peterson C, Ratan RR, Shelanski ML, Goldman JE (1986) Cytosolic free calcium and cell spreading decrease in fibroblasts from aged and Alzheimer donors. Proceedings of the National Academy of Sciences 83: 7999-8001.
78. María Berrocal, Isaac Corbacho, María Vázquez-Hernández, Jesús Ávila, M Rosario Sepúlveda, et al. (2015) Inhibition of PMCA activity by tau as a function of aging and Alzheimer's neuropathology. Biochim Biophys Acta 1852: 1465-1476.
79. Laura Contreras, Paulino Gomez-Puertas, Mikio Iijima, Keiko Kobayashi, Takeyori Saheki, Jorgina Satrústegui, et al. (2007) Ca^{2+} Activation kinetics of the two aspartate-glutamate mitochondrial carriers, aralar and citrin: role in the heart malate-aspartate NADH shuttle. J Biol Chem 282: 7098-7106.
80. Boerries M (2007) Ca 2+ -Dependent Interaction of S100A1 with F 1 -ATPase Leads to an Increased ATP Content in Cardiomyocytes. Mol Cell Biol 27: 4365-4373.
81. Niescier RF, Hong K, Park D, Min KT (2018) MCU Interacts with Miro1 to Modulate Mitochondrial Functions in Neurons. J Neurosci 38: 4666-4677.
82. Nguyen TT (2014) Loss of Miro1-directed mitochondrial movement results in a novel murine model for neuron disease. Proc Natl Acad Sci USA 111: E3631-E3640.
83. López-Doménech G (2018) Miro proteins coordinate microtubule- and actin-dependent mitochondrial transport and distribution. EMBO J 37: 321-336.
84. Mitchell L, Reda KE, Fatima H, Vasquez CE, Quintero-Carmona OA (2021) TRAK proteins encode distinct MIRO-dependent and MIRO-independent mechanisms for associating with the mitochondrial outer membrane. Biorxiv https://www.biorxiv.org/content/10.1101/2021.06.03.446977v1.
85. Hajnóczky G (2014) Reliance of ER-mitochondrial calcium signaling on mitochondrial EF-hand Ca^{2+} binding proteins: Miros, MICUs, LETM1 and solute carriers. Curr Opin Cell Biol 29: 133-141.
86. Pera M, Söderbom G, Esterline R, Oscarsson J, Mattson MP, Eds (2020) Chapter Nine - MAM and C99, key players in the pathogenesis of Alzheimer's disease in International Review of Neurobiology, Metabolic and Bioenergetic Drivers of Neurodegenerative Disease: Neurodegenerative Disease Research and Commonalities with Metabolic Diseases. Academic Press 235-278.
87. Area-Gomez E (2012) Upregulated function of mitochondria-associated ER membranes in Alzheimer disease. EMBO J 31: 4106-4123.
88. Wolfe LA, Morava E, He M, Vockley J, Gibson KM (2012) Heritable disorders in the metabolism of the dolichols: A bridge from sterol biosynthesis to molecular glycosylation. Am. J. Med. Genet 160: 322-328.
89. Guillén-Samander A, Marianna Leonzino, Michael G Hanna, Ni Tang, Hongying Shen (2021) VPS13D bridges the

ER to mitochondria and peroxisomes via Miro. J Cell Biol 220: 202010004.

90. Kornmann B, Osman C, Walter P (2011) The conserved GTPase Gem1 regulates endoplasmic reticulum-mitochondria connections. Proc Natl Acad Sci USA 108: 14151-14156.

Supplementary Information

Detailed Materiel and Method

Cell Culture & Bioenergetics

Primary human fibroblasts were all free of mycoplasma by routine screening and were cultured in phenol-red free Dulbeco's modified essential medium, containing 1 g/l glucose supplemented with charcoal stripped 10% fetal bovine serum (Gibco ThermoFisher), 20 m M pyruvate, 2 mM glutamate (M1). Healthy fibroblasts originated from a clinical biopsy obtained in a 54yo male, AD fibroblasts from a 50yo Caucasian male. When appropriate, AD fibroblasts were treated for 2-hours with SPP used at 0.0002%, 0.001% or 0.005%. When metabolic challenges were needed cells were grown in a glucose free medium (M2) or in a glucose free medium containing a carnitine palmitoyltransferase 1 inhibitor (M3) for 24h prior to the experimentation. Bioenergetic studies were carried out in M1, M2 and M3 using the BBS technology (ICDD-sas, France).

Image Capture & Analysis

Widefield epifluorescence microscopy was performed on live fibroblasts using a digital microscopy workstation Axioplan II (Zeiss, Germany) fitted with a cooled CCD camera (Sensicam; Cooke) and a high-speed wavelength switcher (model Lambda DG4; Sutter Instruments) driven by the Intelligent Imaging Innovation automation (Everest workstation, 3i). Mitochondria were labeled with Mitotracker green (ThermoFisher) excited at excited at 488 nm. For mitochondrial motility assessment, time-lapse image stacks (up to 5 optical sections, 0.2 µm z-spacing), at 0.23 µm per pixel, 350 ms per stack, were collected every 10sec, for a total of 6 minutes per cell. In normal cells, we observed limited changes in fluorescence intensity, not causing phototoxicity or modifying cell activity levels, or mitochondrial motility levels with time under these conditions. Mitochondrial motility was analyzed by the Mitostream® software v1.2 (ICDD, France). For immunocytochemical staining, cells were fixed for 20 min with 4% paraformaldehyde in PBS, and permeabilized with 0.5% triton-X in PBS for 15 min. The cells were then incubated with primary antibodies for 1 h. Fluorescent proteins such as Congo Red, and Alexa fluor 456, were exited at 456nm, GFP, Picogreen and Alexa fluor 488 at 488nm. Nucleais were counterstained using cell permeant Hoechst, excited at 350nm. Computer aided image analysis of acquired fluorescent images was performed with the Slidebook software v3.4 (3i, USA).

mtDNA Content Assessment

MtDNA staining in live cells was achieved by diluting stock PicoGreen solution at 3 µl/ml (1 – 3 h). The cells were rinsed three times and visualized using an epifluorescent microscope. Quantification of mtDNA content using Picogreen was previously described (1).

De Novo Protein Synthesis

We used Click-IT™ L-Homopropargylglycine (Thermofischer) to visualize nascent protein synthesis in cells grown in a L-methionine-free medium. Cells were treated with SPP or with the vehicle for 1h30 min. 50µM L-Homopropargylglycine was co-incubated with the treatment for 30 min. Cells were washed in PBS and immediately fixed in 3.7% formaldéhyde; 3% BSA et 0.5% Triton® X-100 for 15minutes and permeabilized in Triton X100 0.5% for another 20 min. Click-IT chemistry was performed according to manufacturer recommendations. Nuclei were counterstained with DAPI.

PERK Signaling

Western Blot analysis for eIF2α et 51Ser-P eIF2α (Cell Signaling) was performed on nitrocellulose membranes transferred from 3 independent electrophoresis gels run using 40ng protein extracted from the different experimental conditions in RIPA buffer. All gels were stripped and reprobed with either eIF2α or Ser51-P eIF2α antibody depending on the initial dual labeling with either eIF2α or Ser51-P eIF2α antibody and α-tubulin. All membranes were imaged and analyzed on an Amersham680.

Amyloid Beta Fibrils and Tau / P-Tau Immunocytochemistry

Amyloid-β fibrils were evaluated by Congo red staining. The extracellular fibrils were evaluated under the fluorescent microscope (Zeiss) at 40× magnification with excitation wavelength λmax 530–585 nm and emission above λmax 600nm (2). Immunostaining with Tau, and Ser396 P-Tau antibodies was performed on cells cultured on glass coverslips and fixed with 4% paraformaldehyde for 20 min at 25°C and then incubated overnight at 4°C with primary antibodies. The immunoreactivity was probed with Alexa-546- or Alexa-488-conjugated goat anti-mouse or anti-rabbit secondary antibodies. DAPI was used for the nuclear counterstaining.

Proximity Ligation Assay (PLA):

Specific primary antibody for SERCA-II and GRP75 are reference in the resource table I in supplementary information. PLA in situ red mouse/goat kit was purchased from Duolink (Sigma Aldrich). This kit includes mouse and goat secondary antibodies with probes, blocking solution, wash buffers A and B, amplification solution, ligase solution and detection reagent.

Electron Microcopy

Fixation was done with 2% paraformaldehyde, 2.5% glutaraldehyde in 0.1 M sodium cacodylate overnight at 4 °C. Samples were contrasted with osmium tetroxyde (2%) in 0.2 M sodium cacodylate for 1h on ice. Samples were washed for 10 min with 0.1 M sodium cadodylate on ice, followed by an overnight incubation in 2% uranyl acetate in H_2O at 4 °C. Samples were progressively dehydrated they were then incubated in increasing concentrations of resin. Cells embedded in resin were then cut in ultra-thin sections of 75 nm using a microtome. Samples cut in ultra-thin slices were contrasted a second time with 2% uranyl acetate for 5 min followed by incubation for 2.5 min in a freshly made lead citrate solution. Imaging was carried out on transmission electron microscope FEI Morgagni 120 kV.

Citation: Giorgio Dell'Acqua, Tony McFadden, Beatrice Blanc, Romain MJ Lasseur, Nicolas Brouilly, et al. (2025) Plant Polyprenols Disrupt the IP3R-GRP75-VDAC-MCU Axis to Restore Mitochondrial Motility Defects Associated with Alzheimer's Disease. Journal of Alzheimer's Disease & Reports. SRC/JADR-111.
DOI: doi.org/10.47363/JADR/2025(2)110

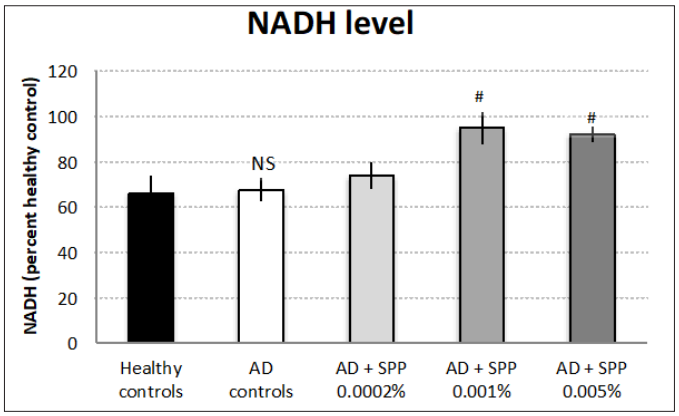

Figure S1: SPP Generated a Dose-Dependent Increase in NADH Production

Effect of SPP treatment on NADH production in cells grown in a medium depleted in glucose and containing a carnitine palmitoyltransferase 1 inhibitor. This result indicate that SPP promotes respiration from substrates such as glutamate/malate, pyruvate/malate, palmitoylcarnitine/malate, and succinate/rotenone. Analysis done at the level of cell culture wells (n=60).

###p<0.001, ##p<0.001, #p<0.05 indicate significant differences comparing untreated AD-cells to SPP-treated AD-cells . Error bars are SD.

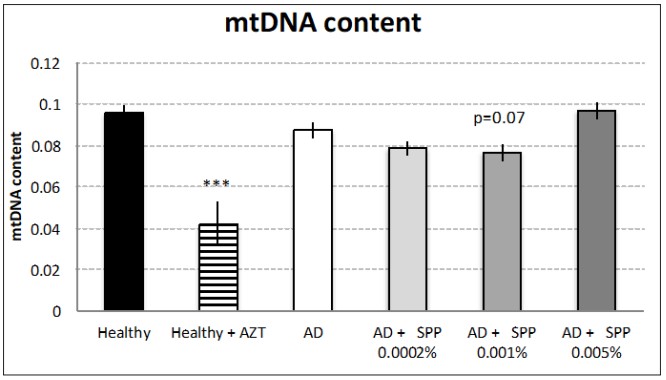

Figure S2: Treatment with SPP did not Modify mtDNA Content

Quantification of mtDNA content in the different experimental populations (Analysis done at the cellular level, n=186, 3 independent replicates). Depletion of mtDNA content was significant when healthy cells were incubated with 10µM AZT, validating the experiments. mtDNA content was not modified by AD nor by SPP treatment of AD cells.

***p<0.0001, **p<0.001, *p<0.05 indicate significant differences comparing healthy controls to other experimental groups. Error bars are SEM.

Table S1: List of Chemical and Antibodies Used in This Study

Resource	Usage	Description	Supplier	Reference
Chemical	Bioenergetics	BBS kit	ICDD	b-IC3002
Chemical	LCI	Mitotracker Green	InVitrogen	M7514
Chemical	LCI	Hoechst	InVitrogen	H1399
Chemical	ICC	DAPI	InVitrogen	D1306
Chemical	LCI	Congo Red	Sigma Aldrich (Merck)	C6767
Primary AB	ICC	Tau (Clone5)	ABCam	AB80579
Primary AB	ICC	P-tau (S396)	ABCam	AB109390
Secondary AB	ICC	Alexa-546	Gibco	A10040
Secondary AB	ICC	Alexa 488	ABCam	AB150113
Primary AB	WB	αtubulin	Cell signaling	#3873
Primary AB	WB	Ser51-Phospho-eiF2α	Cell signaling	#3398
Primary AB	WB	eiF2α	Cell signaling	#9722
MW Ladder	WB	ECLαdualValue®		
markers	General Electric	RPN810		
Secondary AB	WB	Detection kit	General Electric	RPN2108
Chemical	WB	ECL® prime	General Electric	RPN2232
Chemical	CC	Click-IT™ L-Homopropargylglycine (HPG)	ThermoFischer SCI	C10186
Primary AB	PLA	SERCA II ATPase	ABCam	AB3625
Primary AB	PLA	GRP75	ABCam	AB2799
Chemical & secondary AB	PLA	DuoLink starter	Sigma Aldrich (Merck)	DUO92101

LCI = Live Cell Imaging, ICC = Immunocytochemistry, W= Western Blot, CC= Click Chemistry, PLA= Proximity Ligation Assay

References

1. Ashley N, Harris D, Poulton J (2005) Detection of mitochondrial DNA depletion in living human cells using PicoGreen staining. Exp Cell Res 303: 432-446.
2. Clement CG, Truong LD (2014) An evaluation of Congo red fluorescence for the diagnosis of amyloidosis. Hum Pathol 45: 1766-1772.